

Nitrogen Bubbles at Pt Nanoelectrodes in Non-Aqueous Medium-Oscillating Behavior and Geometry of Critical Nuclei

Qianjin Chen, Yuwen Liu, Martin A. Edwards, Yulong Liu, and Henry S. White

Anal. Chem., **Just Accepted Manuscript** • DOI: 10.1021/acs.analchem.9b05510 • Publication Date (Web): 13 Apr 2020

Downloaded from pubs.acs.org on April 17, 2020

Just Accepted

“Just Accepted” manuscripts have been peer-reviewed and accepted for publication. They are posted online prior to technical editing, formatting for publication and author proofing. The American Chemical Society provides “Just Accepted” as a service to the research community to expedite the dissemination of scientific material as soon as possible after acceptance. “Just Accepted” manuscripts appear in full in PDF format accompanied by an HTML abstract. “Just Accepted” manuscripts have been fully peer reviewed, but should not be considered the official version of record. They are citable by the Digital Object Identifier (DOI®). “Just Accepted” is an optional service offered to authors. Therefore, the “Just Accepted” Web site may not include all articles that will be published in the journal. After a manuscript is technically edited and formatted, it will be removed from the “Just Accepted” Web site and published as an ASAP article. Note that technical editing may introduce minor changes to the manuscript text and/or graphics which could affect content, and all legal disclaimers and ethical guidelines that apply to the journal pertain. ACS cannot be held responsible for errors or consequences arising from the use of information contained in these “Just Accepted” manuscripts.

Nitrogen Bubbles at Pt Nanoelectrodes in Non-Aqueous Medium-Oscillating Behavior and Geometry of Critical Nuclei

Qianjin Chen ^{a*}, Yuwen Liu ^b, Martin A. Edwards ^c, Yulong Liu ^a and Henry S White ^{c*}

^aKey Lab of Science and Technology of Eco-Textile, Ministry of Education, College of Chemistry, Chemical Engineering and Biotechnology, Donghua University, Shanghai, 201620, China

^bCollege of Chemistry and Molecular Sciences, Wuhan University, Wuhan, 430072, China

^cDepartment of Chemistry, University of Utah, Salt Lake City, Utah, 84112, United States

ABSTRACT: Gas bubble evolution are omnipresent in many electrochemical and photoelectrochemical processes. We previously reported the formation of individual H₂, N₂ and O₂ nanobubbles generated from electrocatalytic reduction of H⁺, oxidation of N₂H₄ and H₂O₂, respectively, at Pt nanodisk electrodes in the aqueous solution. All the nanobubbles formed display a dynamic stationary state of three phase boundary with an invariant residual current. Here we test the hypothesis that gas nanobubbles can also be electrogenerated in non-aqueous medium. Interestingly, we found oscillating bubble behavior corresponding to nucleation, growth and dissolution in dimethylsulfoxide and methanol. One possible explanation of the oscillation mechanism is provided by the instable dynamic equilibrium between the gas influx due to supersaturation and outflux due to Laplace pressure. Furthermore, the critical gas concentration for N₂ nanobubble nucleation are estimated to be 148, 386, 200 and 16 times supersaturation and the contact angle of critical nuclei to be 164, 151, 160, and 174° in water, dimethylsulfoxide, ethylene glycol and methanol, respectively. This is the first report on electrochemical nucleation of gas bubbles in non-aqueous solvents. Our electrochemical gas bubble study based on nanoelectrode platform has proven to be a prototypical example of single-entity electrochemistry.

INTRODUCTION

Gas-evolution is important to many electrocatalytic process, such as chlorine-alkali process,¹⁻² H₂ and O₂ production from water splitting,³⁻⁴ and CO₂ and N₂ from electro-oxidation in fuel cells (such as methanol and hydrazine).⁵⁻⁶ It is known that the formed gas bubbles on electrode surface will increase the Ohmic resistance and reduce electrolysis efficiency.⁷⁻⁸ Management of these interfacial gas bubbles inherently requires a better understanding of bubble evolution including nucleation, growth and detachment. Several analytical techniques have been introduced to study the individual nanoscale bubble at interface as well as in the liquid phase.⁹ Atomic force microscopy (AFM) is most popular technique and provides the earliest evidence on the existence of surface nanobubbles,¹⁰⁻¹¹ however, it suffers from very limited temporal resolution, which is critical for bubble dynamics study. The optical microscopy is a nonintrusive and direct method with balanced temporal and spatial resolutions. Fluorescence microscopy has been utilized to monitor the dynamic nucleation and growth of gas nanobubbles from solvent exchange¹² and electrocatalytic water splitting.¹³ Super-resolution dark-field microscopy¹⁴⁻¹⁵ and surface plasmon resonance microscopy¹⁶⁻¹⁸ are also appropriate for the visualization of interfacial nanobubble dynamics. These studies allow the evaluation of catalytic activity of individual nanocatalysts and provides new ideas to elucidate heterogeneous nucleation process of nanobubbles. On the other hand, advanced electrochemical methods have excellent temporal resolution and current sensitivity for single gas nanobubbles. Ying and Long et al. employed the patch clamp technique to measure the formation and growth time of single H₂ nanobubble from NaBH₄ hydrolysis through a nanopore confinement.¹⁹ The scanning

probe electrochemistry, a technique utilizing glass nanopipettes to create nanoscale dimension electrode surface, has been successfully adopted to probe and quantify the nucleation and bubble behavior on Pt surface.²⁰⁻²¹

Previously, we developed nanoelectrode method for the electrogeneration of individual H₂, N₂ and O₂ nanobubbles, where gas molecules are electrogenerated by reduction or oxidation of a species yielding gas product. For example, an individual N₂ nanobubble can be formed at a Pt nanoelectrode by hydrazine oxidation, creating a highly N₂ gas supersaturated solution around the electrode surface, leading to a bubble nucleation.²² Similarly, an individual H₂ nanobubble can be formed at Pt, Au and Pd nanoelectrodes by electroreduction of proton,²³⁻²⁶ while an individual O₂ nanobubble can be generated by oxidation of water²⁵ or hydrogen peroxide.²⁷ Among all these electrogenerated gas bubbles, the nucleation is indicated by a sharp current drop to a small but nonzero current in the voltammetry. The gas nanobubble blocks almost all the electrode surface and the detected residual current stays invariant when the potential is further scanned, suggesting a dynamic equilibrium between the gas dissolution and re-generation.²⁸ Based on this nanoelectrode platform, the critical concentration necessary for gas nucleation,^{22-23, 27} bubble nucleation rate,²⁹⁻³⁰ as well as the geometry of critical bubble nuclei³¹ have been successfully measured.

Noted that for all the previous electrochemical study of nanobubbles, the solution medium is limited to water. We speculated that the metal electrode surface must be sufficiently hydrophobic for the gas nanobubble to remain tightly pinned. Manipulation of gas/electrode/solution interaction could obtain very different surface energetics that possibly lead to different bubble dynamics. Herein, based on this nanoelectrode platform, we reported an interesting bubble oscillation behavior in non-

aqueous solution and measured the critical concentration for nucleation, and the nanoscopic geometry of critical nuclei at single nucleation level. Specifically, N₂ bubble from hydrazine oxidation was chosen for the case study because the mechanism and kinetics of the electrode reaction on Pt have been previously investigated³²⁻³⁴ and anhydrous hydrazine is commercially available and directly used for solution preparation. The non-aqueous solvents chosen need to be miscible with anhydrous hydrazine and relatively electrochemically inert within the potential window for hydrazine oxidation in the experiment. Selected solvents physical properties are listed in Table 1.

Table 1. Physical properties of selected solvents^a

Solvent	H ₂ O	EG	DMSO	MeOH
Viscosity (mPa S)	0.890	16.06	1.987	0.544
Surface tension (mN/m)	72.06	48.02	42.92	22.17
N ₂ solubility (mM)	0.66	0.61 ³⁵	1.17 ³⁶	5.78 ³⁵
N ₂ diffusivity (×10 ⁻⁵ cm ² /s)	1.9	0.11 ^b	0.85 ^b	3.11 ^b

^aAll data taken from Handbook of Chemistry and Physics at 25 °C, except where otherwise referenced.³⁷

^bDiffusivity is calculated from Stokes Einstein equation.

EXPERIMENTAL SECTION

Materials. Sulfuric acid (98%) and anhydrous hydrazine (N₂H₄, 98%) were purchased from Sigma-Aldrich and used as received. All aqueous solutions were prepared using deionized water (18.2 M Ω ·cm). Non-aqueous solvents including dimethylsulfoxide, acetonitrile, dimethylformamide, methanol, ethanol, ethylene glycol, acetone, tetrahydrofuran, 1,4-dioxane, nitromethane and dichloromethane were purchased from Fisher scientific. Ferrocene (98%, Sigma-Aldrich) was purified twice by sublimation. In all the solution prepared, no additional electrolyte was added.

Nanoelectrode Fabrication. Pt nanodisk electrodes were fabricated according to previously reported procedures.³⁸ Details can be found in the literature as well as our previous reports.²³⁻²⁴ A 25 μm diameter Pt wire (Goodfellow Corp. 99.99%) was first electrochemically sharpened, then carefully aligned along the glass capillaries (Dagan Corp. o.d. = 1.65 mm, i.d. = 1.10 mm) and sealed within the glass in H₂ flame. The radii of the nanodisk electrodes, *a*, were determined from the voltammetric steady-state diffusion-limited current, *i*_{lim}, for the oxidation of ferrocene (Fc → Fc⁺ + e⁻) dissolved in acetonitrile (CH₃CN) containing 0.10 M tetrabutylammonium hexafluorophosphate (TBAPF₆), using the equation:

$$i_{\text{lim}} = 4nFD_{\text{Fc}}C_{\text{Fc}}a \quad (1)$$

where *D*_{Fc} (2.4 × 10⁻⁵ cm²/s) and *C*_{Fc} are the diffusion coefficient and the bulk concentration of Fc, respectively, and *n* is the number of electrons transferred per molecule (= 1 for Fc oxidation). Experimental steady-state voltammograms for measuring the electrode radii are presented in Figure S1 in the Supporting Information.

Electrochemical Measurement. A Dagan Cornerstone Chem-Clamp potentiostat and a Pine RDE4 (used as waveform generator) were interfaced to a computer through a PCI data acquisition card (National Instruments) to collect i-V data. A Ag/AgCl (in 3 M NaCl) electrode and a saturated calomel electrode (SCE) were used as the counter/reference electrode in a two-electrode cell configuration.

Macroscopic Contact Angle Measurement. Macroscopic contact angle of liquid droplet on pre-cleaned bare Pt surface without potential bias was measured by an optical contact angle goniometer

with automatic dispenser (Attension Theta Lite Tensiometer) with 2 μL liquid. The profile of the droplet was recorded using a video camera as shown in Figure S2.

RESULTS AND DISCUSSIONS

The prepared Pt nanoelectrode was first used for the control experiments of H₂ bubble study in 0.5 M H₂SO₄ and N₂ bubble study in 1.0 M N₂H₄ aqueous solution. Typical cyclic voltammetry is shown in Figure 1a and b and is very reproducible over tens of cycles. A peak current of 16.8 nA for H₂ bubble nucleation and 5.8 nA for N₂ bubble nucleation, as well as the essentially stable residual current after bubble formation for a 24 nm radius Pt nanoelectrode is observed, in agreement with our previous results.²²⁻²³

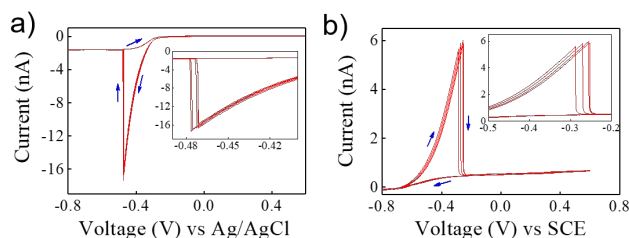


Figure 1. Typical cyclic voltammetry indicating bubble formation at a 24 nm radius Pt disk electrode recorded at a sweep rate of 100 mV/s. (a) H₂ bubble formation in 0.50 M H₂SO₄ aqueous solution with four consecutive cycles. (b) N₂ bubble formation in 1.0 M N₂H₄ aqueous solution with four consecutive cycles.

Electrogeneration of N₂ nanobubble from hydrazine oxidation in nonaqueous solvent were observed in EG, DMSO and MeOH. As shown in Figure 2a, c and e, at low hydrazine concentrations, the current shows a quasi-sigmoidal wave, increasing with increasing overpotential. Compared to the well-defined mass transport limited current response in aqueous solution as demonstrated in earlier report,²² the voltammogram in non-aqueous solution is rather “kinetically” controlled, probably due to the absence of extra charge carrier/supporting electrolyte in solution.^{32, 39} The current is proportional to the hydrazine concentrations, confirming that the possible Faradic current contribution from EG or MeOH oxidation is negligible compared to hydrazine oxidation. Overall, the generated N₂ gas molecules at electrode surface in this scenario is not sufficient to stimulate a stochastic nucleation. As hydrazine concentration further increases to 2.0 M in EG, 3.0 M in DMSO and 1.0 M in MeOH, respectively, as shown in Figure 2b, d and f, precipitous current drop corresponding to bubble nucleation and growth is observed. Specifically, the hydrazine oxidation current decreases from 1.07 nA to a residual current of 0.1 nA at a potential of 0.20 V vs SCE with 2.0 M N₂H₄ in EG, while the current drops from 7.8 nA to 0.5 nA at 0.22 V with 3.0 M N₂H₄ in DMSO, and from 5.5 nA to 2.5 nA at 0.33 V with 1.0 M N₂H₄ in MeOH, respectively. Moreover, the peak current corresponding to bubble nucleation is found essentially invariant with increasing hydrazine concentration (e.g., 1.07, 0.92 and 0.87 nA for 2.0, 3.0 and 5.0 M N₂H₄ in ethylene glycol, respectively) and the peak potential shifts to lower overpotential due to higher transport flux at higher hydrazine concentration. At low scan rates, the concentration of dissolved gas around the nanoelectrode is maintained at a steady state due to the rapid mass transport at nanoelectrodes (see Figure S3 for scan rate independence of voltammograms). Thus the surface concentration of dissolved gas prior to nucleation is directly proportional to the current by:

$$C^{\text{surf}} = \frac{i}{4nFDa} \quad (2)$$

where *n* is the number of electrons transferred per gas molecule

(= 4 for N_2), F is Faraday's constant, D is the diffusion coefficient of gas molecule in the solution (see Table 1), and a is the radius of nanoelectrode.

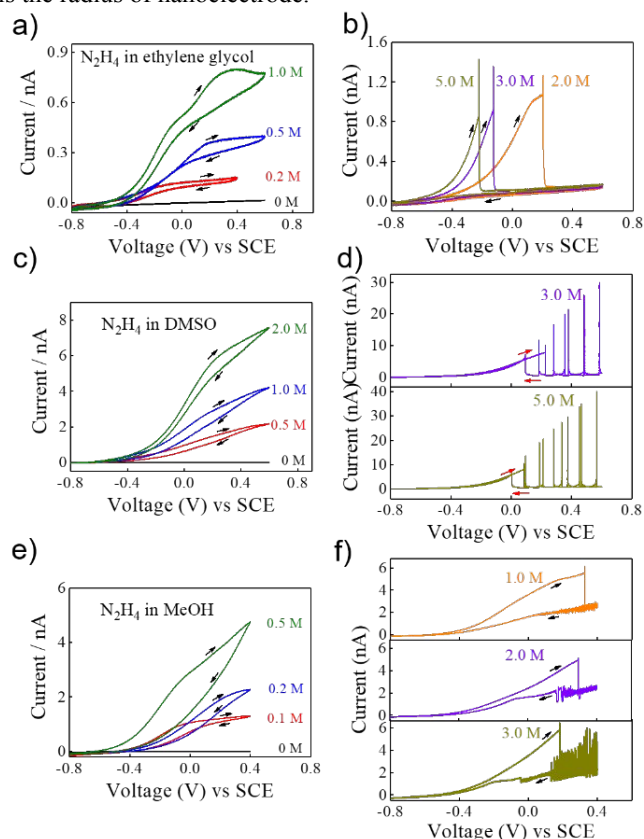


Figure 2. Typical cyclic voltammetry of hydrazine oxidation at a 24 nm radius Pt disk electrode recorded at a sweep rate of 100 mV/s. (a, b) N_2H_4 in ethylene glycol, (c, d) N_2H_4 in DMSO, (e, f) N_2H_4 in methanol with concentrations as indicated. The arrows indicate the direction of forward and backward scan.

A current overshoot prior to current drop is often observed in nonaqueous solvents, as indicated in Figure 2b, d and f. Careful investigation shows such a current overshoot is also general for N_2 bubble nucleation in aqueous solution when high temporal resolution data sampling was used (Figure S4). We speculate such current overshoot originates from the Faradic current due to enhanced hydrazine mass transport at the nanoelectrode accompanying the phase transition (see Figure S5). We take the value prior to the overshoot as the critical current for bubble nucleation quantification. Upon bubble formation, an essentially invariant residual current is observed with N_2H_4 in EG in Figure 2b, suggesting very similar gas nanobubble stabilization as in the aqueous solution. For the cyclic voltammetry in DMSO as shown in Figure 2d, the current responses show oscillating current after bubble is formed. As the potential scans back to negative, the small residual current suddenly increases, indicating the nanobubble is rapidly dissolved and electrode surface is fully re-exposed. As for

methanol in Figure 2f, the current after nanobubble formation displays rigorous variations and such noisy becomes significant for 3.0 M N_2H_4 in MeOH.

To disclose more details, high temporal resolution current time traces at 20 kHz sampling rate corresponding to Figure 2d with 3.0 M N_2H_4 in DMSO is presented in Figure 3a. For comparison, a parallel current time trace with 3.0 M N_2H_4 in ethylene glycol is shown in Figure 3b where no oscillation is associated with N_2 nanobubble. Zoom-ins of bubble nucleation and partial current oscillations in DMSO are shown in Figure 3c. Initially, the N_2 molecules are continuously generated from hydrazine oxidation (state ①). Once $C_{N_2}^{surf}$ is sufficiently high,

stochastic nucleation of a bubble occurs and a small bubble nuclei forms at the electrode surface (state ②). Due to thermodynamically favorable bubble growth, the bubble quickly covers almost the whole electrode surface (state ③). Afterwards, the bubble continues to expand with increasing contact angle from gas side (state ④), until the bubble breaks and dissolves into the solution. The growing of gas bubble with increasing volume and inner contact angle, but with invariant residual current was previously predicted by molecular simulations.⁴⁰ This gas nucleation, growth and dissolution cycle occurs repeatedly as long as high supersaturation can be achieved. Corresponding schematic of bubble dynamic is shown in Figure 3d. Eventually, when the potential scans to less than 0.10 V vs SCE at 16.45s in Figure 3a, the N_2 generation from hydrazine oxidation can no longer balance the bubble and it suddenly shrinks and dissolves (in less than 1 ms) without subsequent bubble nucleation. At this moment, the electrode surface is the same as state ① prior to nucleation. Additional current time trace with bubble oscillation and their zoom-ins for 3.0 M N_2H_4 in MeOH are provided in the Supporting Information (Figure S6).

While Figure 2d and Figure S7 in the Supporting Information clearly shows the bubble oscillation behaviour is related with N_2H_4 concentration, studies at different scan rate in Figure 4a-4d display the oscillation behaviour diminishes with increasing scan rates. At scan rate as high as 1000 mV/s, only the bubble nucleation and dissolution is observed. At low scan rate of 40 mV/s, Figure 4a shows periodic bubble oscillation with the peak current proportional to scan potential. This correlation is confirmed by experiments of bubble oscillation at constant potential applied (Figure 4e-i). While the oscillation frequency increases slightly from 1.36 s^{-1} at 0.05 V to 1.64 s^{-1} at 0.60 V vs SCE, and the average bubble nucleation and growth time decreases with increasing potential (Figure S8). Considering that optical techniques for such nanobubbles dynamics at nanoelectrodes is extremely challenging, if not possible, we further consider the noise spectrum of the current oscillation from Figure 4e-h. Figure S9 shows the power spectral densities of current signal at different potentials. A main peak at approximately 1.5 Hz indicates the periodic bubble release at nanoelectrode. As the potential increases, this peak shifts to higher frequency with lower power densities, indicating faster bubble oscillation due to faster gas generation, consistent with previous results of the overpotential fluctuation at a gas evolving microelectrode with constant current density.⁴¹

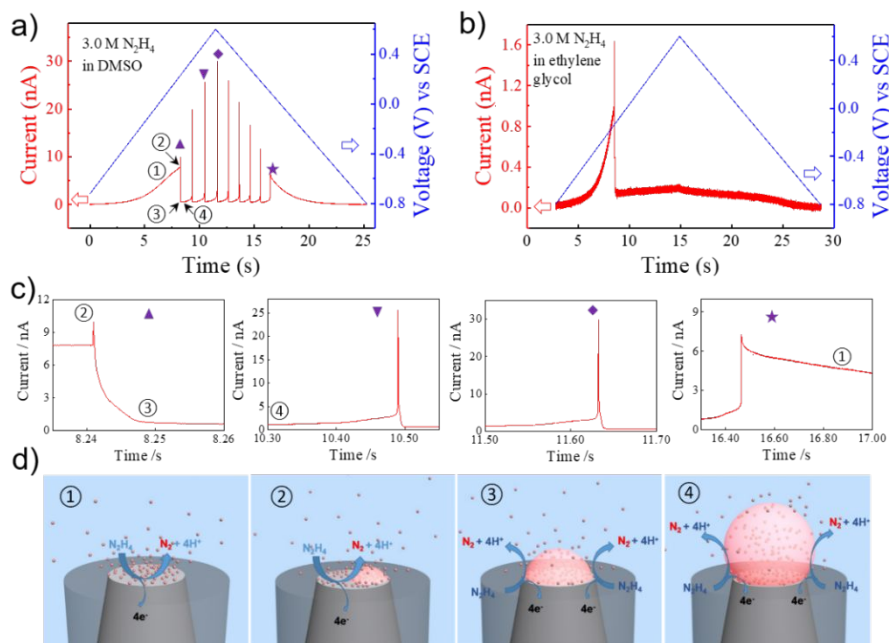


Figure 3. High temporal resolution current traces of voltammetric responses at scan rate of 100 mV/s and sampling rate of 20 kHz (a) in 3.0 M N_2H_4 DMSO solution with bubble oscillation, (b) in 3.0 M N_2H_4 ethylene glycol solution without current oscillation. The red and blue curves stand for the current and potential, respectively. (c) Zoom-ins of four current oscillation peaks from (a) as indicated by different symbols (\blacktriangle , bubble nucleation, \blacktriangledown and \blacklozenge , two typical oscillation, \star , bubble dissolution). (d) Schematics for different states of bubble, ①bare electrode, ②bubble nucleation, ③growth and ④expanding.

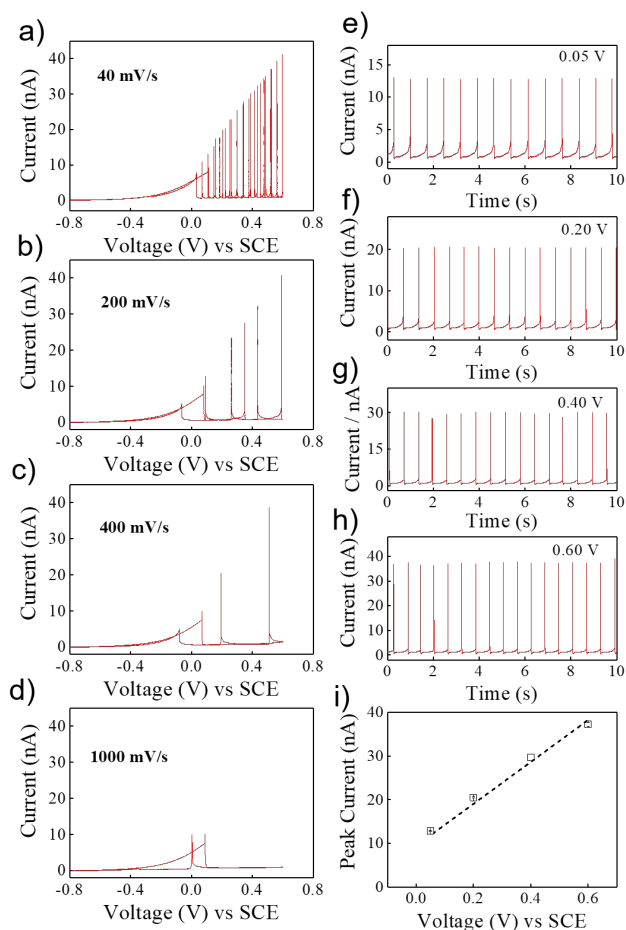


Figure 4. Typical cyclic voltammetry of N_2 bubble oscillation at a 24 nm radius Pt disk electrode in 5.0 M N_2H_4 in DMSO solution as a function of different scan rate (a-d) 40, 200, 400, and 1000 mV/s. Typical current time traces of bubble oscillation at different potential applied (e-h) 0.05, 0.20, 0.40 and 0.60 V vs SCE. Oscillation peak

currents as a function of potential (i). All the measured are recorded at a sampling rate of 20 kHz.

We now consider possible reasons contributing to the oscillating behavior of nanobubbles observed in DMSO and MeOH. Conventional gas nanobubbles pinned on the surface have been found to have extraordinary long lifetime and unusual small contact angles (from gas side).^{10, 42-44} Gas supersaturation and contact line pinning are proposed to explain the stabilization of nanobubbles.⁴⁵⁻⁴⁷ Lohse and Zhang speculated the contact angle of a surface nanobubble is set by the equilibrium between gas influx due to oversaturation and gas outflux due to the Laplace pressure.⁴⁶ At equilibrium, $\sin\theta_c = \zeta L / L_c$, where L is the nanobubble contact length with critical contact length of $L_c = 4\gamma / P_0$, and ζ is the oversaturation. In the case of nanobubble electrogeneration in water as shown in Figure 1, upon nucleation, the bubble pinned on the electrode will grow aggressively and the contact angle (from gas side) increases. When more and more electrode surface are covered by the bubble, the electrode edge available for gas electrogeneration will decrease, causing a reduction of gas influx into the gas bubble. Due to strong contact line pinning of gas nanobubble on hydrophobic electrode surface, the dynamic equilibrium between the gas influx and outflux can always be sustained. However, in the case of non-aqueous medium, the pinning of gas nanobubble on electrode can be much weaker due to the very different surface energetics. This weaker gas nanobubbling pinning on electrode surface consequently causes nanobubble shape instability and easier break of the equilibrium between gas influx and outflux, eventually leading to the bubble oscillation behavior. Note that in our previous study of H_2 nanobubble from proton reduction in aqueous solution in the presence of surfactants (Triton X-100, TEGME and CTAB), a similar current oscillation was not observed.²³ We speculate that while the surfactant molecules will certainly decrease liquid surface tension and lead to a different surface energetics at the three phase interface, the surfactant molecules adsorbed at the liquid/gas interface will also play a role to mechanically strengthen the nanobubble shape and kinetically slow down

diffusive outflux of gas from nanobubble, both of which can stabilize a surface nanobubble. We believe such shape instability is an overall consequence of several complicated surface processes including gas bubble wetting on electrode/glass surface interface, electrochemical reaction at three phase boundary, and gas diffusion around surface bubble. Possible nanobubble coalescence process prior to bubble detachment cannot be excluded. Systematic evaluation of this current oscillatory behaviour in experimental conditions is certainly further needed in order to identify the detailed mechanism. Eventually, unlike in DMSO and MeOH, the oscillating bubbles in EG is not typical as shown in Figure 2b. We speculate this is due to the extremely high viscosity of EG, which could kinetically trap an oscillating bubble dynamics.

Many more non-aqueous solvents have been tested (Table S1 for the whole list), however, the well-defined peak shaped voltammogram corresponding to bubble nucleation are not always observed, due to possible solvent electrooxidation and bubble instability. We limit our electrochemical analysis of N₂ gas bubble to the four different solvents as listed in Table 1. Figure 5a shows the typical voltammetric response of N₂ bubble formation from hydrazine oxidation in DMSO with different radius of Pt nanoelectrodes. Regardless the current oscillations, the peak feature and peak current values are very reproducible (see Figure S3 for multiple scan cycles of cyclic voltammetry in different solvents). Figure 5b summarizes the peak current value for N₂ bubble nucleation, i_{nb}^p , as a function of electrode radius in four different solvents, and a linear relationship based on equation 2 is adopted. The N₂ molecule diffusivity in the non-aqueous solvent is estimated from their liquid viscosity based on Stokes Einstein equation (Table 1), while D_{N_2} in water is taken as 1.9×10^{-5} cm²/s.⁴⁸ From the slope of linear fit (0.301 ± 0.009 for water, 0.040 ± 0.002 for EG, 0.462 ± 0.032 for MeOH and 0.326 ± 0.007 for DMSO) in Figure 5b, the critical surface concentration of N₂, C_{crit} , for bubble nucleation, were estimated to be 98 ± 5 mM, 236 ± 12 mM, 234 ± 5 mM, and 91 ± 6 mM, in water, EG, DMSO, and MeOH, respectively. These overall concentration corresponds to an ~ 148 , ~ 386 , ~ 200 , and ~ 16 times supersaturation of the N₂ gas saturation value at room temperature and atmospheric pressure for each solvent as summarized in Table 2. Meanwhile, the critical concentration and supersaturation values for individual nanoelectrodes are also calculated and presented in Figure 5c and 5d. Results are consistent from linear fit. For the three non-aqueous solvents, DMSO, EG and MeOH, we found the supersaturation for N₂ bubble nucleation is correlated with liquid surface tension while water is excepted (Figure S13, Supporting Information).

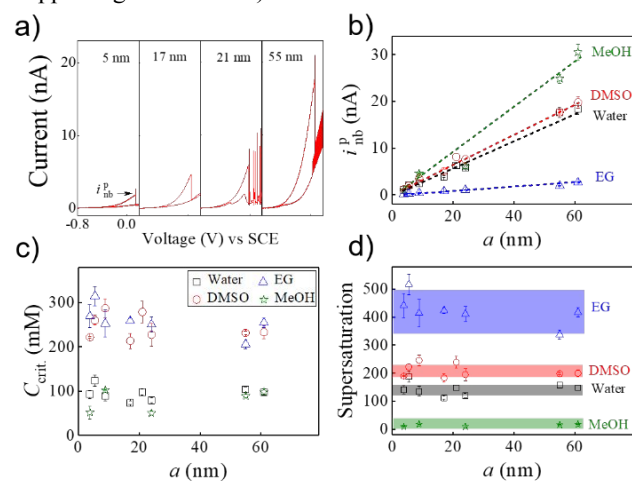


Figure 5. (a) Typical i - V responses of Pt nanoelectrodes with radii of 5, 17, 21 and 55 nm in 5.0 M N₂H₄ DMSO solution at a scan rate of 100 mV/s. Potential window was limited in order to clarify the peak shape voltammetric response. (b) Nanobubble peak current, i_{nb}^p , (c) critical N₂ concentration for bubble nucleation calculated from eq 2, C_{crit} , and (d) critical supersaturation for bubble nucleation, $S(C_{crit.}/C_0)$, based on the solubility from Table 1 as a function of electrode radius in different solvent mediums. Error bars are based on the voltammetric response from multiple measurement with the same electrode. The lines and colored bands are drawn to guide the eye.

Table 2. Contact angle from liquid side in a macroscopic liquid droplet, oscillating bubble behaviour, critical gas concentration, $C_{crit.}$, critical supersaturation, S , for bubble nucleation, contact angle from liquid side and radius of curvature of critical nuclei in the selected solvents. No obvious correlation between the macroscopic and nanoscopic angles is seen.

Solvent	H ₂ O	EG	DMSO	MeOH
θ of liquid droplet (deg.)	58	44	31	20
Oscillation behavior	No	Rarely ^a	Yes	Yes
$C_{crit.}$ (mM)	98±5	236±12	234±5	91±6
$S(C_{crit.}/C_0)$	148±8	386±20	200±4	16±1
θ of critical nucleus (deg.) ^b	164±1	151±2	160±2	174±2
$r_{curv.}$ (nm)	9.7	2.5	4.3	27.7

^aTypical example and features is shown in Figure S11 and S12.

^bEstimation from voltammetric measurement on individual nanoelectrodes.

In classical nucleation theory for a bubble, the rate of nucleation, J , is expressed as⁴⁹

$$J = J_0 \exp\left(-\frac{16\pi\gamma^3\Phi(\theta)}{3k_B T(P_{gas} - P_0)^2}\right) \quad (3)$$

where J_0 is the pre-exponential factor; γ is the surface tension of solvent-gas interface; $\Phi(\theta) = (2 - \cos\theta)(1 + \cos\theta)^2/4$ is the geometric factor and is a function of the contact angle θ from liquid side. P_{gas} is the pressure of the gas inside the critical nucleus and P_0 is the ambient pressure. Based on the distribution of nucleation peak currents from independent voltammetric measurement, the pre-exponential factor, J_0 , and the properties of single critical nuclei such as contact angle, θ , can be extracted based on a previous developed statistical model.³¹ With known critical nuclei internal pressure P_{gas} and assuming an equilibrium between the solution and the bubble nuclei, the radii curvature of the critical nuclei, is calculated from the Young-Laplace equation, $r_{curv} = 2\gamma/(P_{gas} - P_0)$. Details of θ and r_{curv} of critical nuclei pertaining to bubble nucleation in different solvents is summarized in Table 2. Interestingly, the estimated nanoscopic contact angles from liquid side of critical nuclei in the non-aqueous solvents ($151 \pm 2^\circ$ in EG, $160 \pm 2^\circ$ in DMSO, $174 \pm 2^\circ$ in MeOH) are very close to the value in water ($164 \pm 1^\circ$), but are much higher than the macroscopic contact (58° in H₂O, 44° in EG, 31° in DMSO, 20° in MeOH). These large contact angles of N₂ nanobubbles from liquid side are consistent with previous small contact angle measured from Tapping mode AFM for surface gas nanobubbles.⁵⁰ More interestingly, in our study, the trend of calculated θ of critical nucleus in the four different solvents agrees remarkably well with that of the measured gas oversaturation ($C_{crit.}/C_0 - 1$) based on the model previously proposed by Lohse and Zhang, where the equilibrium contact angle of a surface nanobubble is described by $\sin\theta_e = \zeta L/L_c$.⁴⁶

CONCLUSIONS

In summary, we demonstrated the electrogeneration of single N₂ nanobubbles in different solvent medium. In contrast to the dynamic stationary state of nanobubbles found in aqueous solution, which is indicated by the invariant residual current, the oscillating behavior corresponding to bubble nucleation, growth and dissolution cycle is observed in DMSO and MeOH. We speculate such nanobubble dynamics is probably due to very different contact line pinning of gas nanobubble on electrode surface in the non-aqueous solvents, relative to water. In future work, we will develop this bubble oscillation at nanoelectrodes as a means of revealing the nanoscopic interaction at the gas/liquid/electrode three phase boundary. Based on our nanoelectrode platform for electronucleation, the critical concentration for N₂ bubble nucleation is estimated to be 98, 236, 234 and 91 mM in water, ethylene glycol, DMSO and methanol, respectively, corresponding to 148, 386, 200 and 16 times the saturation concentration. Our unique study of single N₂ nanobubbles also allows quantitative characterization of the geometry of critical nuclei including the contact angle and radius of curvature. Overall, our electrochemical driven gas nanobubble study based on nanoelectrode has proven to be a prototypical example of single-entity electrochemistry.⁵¹

ASSOCIATED CONTENT

Supporting Information. The Supporting Information is available free of charge via the Internet at <http://pubs.acs.org>.

Estimation of nanoelectrode radii, droplet contact angle at Pt plate, effect of scan rate on the voltammograms in different solvent media, current overshoot for gas bubble formation in aqueous solution, possible origin of the current overshoot, potential dependent current oscillation, Zoom-ins of current oscillation in methanol, current oscillation in DMSO, current oscillation in ethylene glycol, list of common solvent media tested in the study. Supersaturation for bubble nucleation in different solvent media

AUTHOR INFORMATION

Corresponding Author

* E-mail: qianjinchen@dhu.edu.cn

* E-mail: white@chem.utah.edu

ACKNOWLEDGMENT

This work was supported by the Office of Naval Research Award No. N00014-16-1-2541. Q.C. acknowledges to the National Science Foundation of China (NSFC-21804018) and Shanghai (19ZR1470800), as well as the start-up funds from Donghua University for support.

REFERENCES

- Karlsson, R. K. B.; Cornell, A., *Chem. Rev.* **2016**, *116*, 2982-3028.
- Moreno-Hernandez, I. A.; Brunschwig, B. S.; Lewis, N. S., *Energy Environ. Sci.* **2019**, *12*, 1241-1248.
- Seh, Z. W.; Kibsgaard, J.; Dickens, C. F.; Chorkendorff, I.; Nørskov, J. K.; Jaramillo, T. F., *Science* **2017**, *355*, eaad4998.
- Jovanović, P.; Stojanovski, K.; Bele, M.; Dražić, G.; Koderman Podboršek, G.; Suhadolnik, L.; Gaberšček, M.; Hodnik, N., *Anal. Chem.* **2019**, *91*, 10353-10356.
- Wasmus, S.; Küver, A., *J. Electroanal. Chem.* **1999**, *461*, 14-31.
- Lu, Z.; Sun, M.; Xu, T.; Li, Y.; Xu, W.; Chang, Z.; Ding, Y.; Sun, X.; Jiang, L., *Adv. Mater.* **2015**, *27*, 2361-2366.
- Harrison, J. A.; Kuhn, A. T., *Surface Technol.* **1983**, *19*, 249-259.
- Faber, M. S.; Dziedzic, R.; Lukowski, M. A.; Kaiser, N. S.; Ding, Q.; Jin, S., *J. Am. Chem. Soc.* **2014**, *136*, 10053-10061.
- Lohse, D.; Zhang, X., *Rev. Mod. Phys.* **2015**, *87*, 981-1035.
- Lou, S.-T.; Ouyang, Z.-Q.; Zhang, Y.; Li, X.-J.; Hu, J.; Li, M.-Q.; Yang, F.-J., *J. Vac. Sci. Technol., B* **2000**, *18*, 2573-2575.
- Ishida, N.; Inoue, T.; Miyahara, M.; Higashitani, K., *Langmuir* **2000**, *16*, 6377-6380.
- Chan, C. U.; Ohl, C.-D., *Phys. Rev. Lett.* **2012**, *109*, 174501.
- Hao, R.; Fan, Y.; Howard, M. D.; Vaughan, J. C.; Zhang, B., *Proc. Natl. Acad. Sci. U. S. A.* **2018**, *115*, 5878-5883.
- Li, S.; Du, Y.; He, T.; Shen, Y.; Bai, C.; Ning, F.; Hu, X.; Wang, W.; Xi, S.; Zhou, X., *J. Am. Chem. Soc.* **2017**, *139*, 14277-14284.
- Zhang, T.; Li, S.; Du, Y.; He, T.; Shen, Y.; Bai, C.; Huang, Y.; Zhou, X., *J. Phys. Chem. Lett.* **2018**, *9*, 5630-5635.
- Fang, Y.; Li, Z.; Jiang, Y.; Wang, X.; Chen, H.-Y.; Tao, N.; Wang, W., *Proc. Natl. Acad. Sci. U. S. A.* **2017**, *114*, 10566-10571.
- Chen, J.; Zhou, K.; Wang, Y.; Gao, J.; Yuan, T.; Pang, J.; Tang, S.; Chen, H.-Y.; Wang, W., *Proc. Natl. Acad. Sci. U. S. A.* **2019**, 201903259.
- Wang, Y.; Chen, J.; Jiang, Y.; Wang, X.; Wang, W., *Anal. Chem.* **2019**, *91*, 4665-4671.
- Hu, Y.-X.; Ying, Y.-L.; Gao, R.; Yu, R.-J.; Long, Y.-T., *Anal. Chem.* **2018**, *90*, 12352-12355.
- Perera, R. T.; Arcadia, C. E.; Rosenstein, J. K., *Electrochim. Acta* **2018**, *283*, 1773-1778.
- Wang, Y.; Gordon, E.; Ren, H., *J. Phys. Chem. Lett.* **2019**, *10*, 3887-3892.
- Chen, Q.; Wiedenroth, H. S.; German, S. R.; White, H. S., *J. Am. Chem. Soc.* **2015**, *137*, 12064-12069.
- Chen, Q.; Luo, L.; Faraji, H.; Feldberg, S. W.; White, H. S., *J. Phys. Chem. Lett.* **2014**, *5*, 3539-3544.
- Luo, L.; White, H. S., *Langmuir* **2013**, *29*, 11169-11175.
- Chen, Q.; Luo, L.; White, H. S., *Langmuir* **2015**, *31*, 4573-4581.
- Chen, Q.; Ranaweera, R.; Luo, L., *J. Phys. Chem. C* **2018**, *122*, 15421-15426.
- Ren, H.; German, S. R.; Edwards, M. A.; Chen, Q.; White, H. S., *J. Phys. Chem. Lett.* **2017**, *8*, 2450-2454.
- Liu, Y.; Edwards, M. A.; German, S. R.; Chen, Q.; White, H. S., *Langmuir* **2017**, *33*, 1845-1853.
- German, S. R.; Edwards, M. A.; Ren, H.; White, H. S., *J. Am. Chem. Soc.* **2018**, *140*, 4047-4053.
- Soto, Á. M.; German, S. R.; Ren, H.; van der Meer, D.; Lohse, D.; Edwards, M. A.; White, H. S., *Langmuir* **2018**, *34*, 7309-7318.
- Edwards, M. A.; White, H. S.; Ren, H., *ACS Nano* **2019**, *13*, 6330-6340.
- Rosca, V.; Duca, M.; de Groot, M. T.; Koper, M. T. M., *Chem. Rev.* **2009**, *109*, 2209-2244.
- Chen, C.-H.; Jacobse, L.; McKelvey, K.; Lai, S. C. S.; Koper, M. T. M.; Unwin, P. R., *Anal. Chem.* **2015**, *87*, 5782-5789.
- Bentley, C. L.; Kang, M.; Unwin, P. R., *J. Am. Chem. Soc.* **2017**, *139*, 16813-16821.
- Battino, R.; Rettich, T. R.; Tominaga, T., *J. Phys. Chem. Ref. Data* **1984**, *13*, 563-600.
- Dymond, J. H., *J. Phys. Chem.* **1967**, *71*, 1829-1831.
- Handbook of Chemistry and Physics*. 97th ed.; CRC Press: Boca Raton, FL, 2016-2017.
- Zhang, B.; Galusha, J.; Shiozawa, P. G.; Wang, G.; Bergren, A. J.; Jones, R. M.; White, R. J.; Ervin, E. N.; Cauley, C. C.; White, H. S., *Anal. Chem.* **2007**, *79*, 4778-4787.
- Kosuke, I., *Electrochemistry in Nonaqueous Solutions*. 2nd ed.; Wiley-VCH: 2010.
- Perez Sirkin, Y. A.; Gadea, E. D.; Scherlis, D. A.; Molinero, V., *J. Am. Chem. Soc.* **2019**, *141*, 10801-10811.

41. Fernández, D.; Maurer, P.; Martine, M.; Coey, J. M. D.; Möbius, M. E., *Langmuir* **2014**, *30*, 13065-13074.
42. Zhang, X.; Chan, D. Y. C.; Wang, D.; Maeda, N., *Langmuir* **2013**, *29*, 1017-1023.
43. Craig, V. S. J., *Soft Matter* **2011**, *7*, 40-48.
44. Alheshibri, M.; Qian, J.; Jehannin, M.; Craig, V. S. J., *Langmuir* **2016**, *32*, 11086-11100.
45. Liu, Y.; Zhang, X., *J. Chem. Phys.* **2014**, *141*, 134702.
46. Lohse, D.; Zhang, X., *Phys. Rev. E* **2015**, *91*, 031003.
47. Tan, B. H.; An, H.; Ohl, C.-D., *Phys. Rev. Lett.* **2017**, *118*, 054501.
48. Cussler, E. L., *Diffusion: Mass Transfer in Fluid Systems*. 2nd ed. ed.; Cambridge University Press: New York, 1997.
49. Blander, M.; Katz, J. L., *AIChE J.* **1975**, *21*, 833-848.
50. An, H.; Liu, G.; Atkin, R.; Craig, V. S. J., *ACS Nano* **2015**, *9*, 7596-7607.
51. Lemay, S. G., *ACS Nano* **2019**, *13*, 6141-6144.

Table of Content

